

Face-Guided Sentiment Boundary Enhancement for Weakly-Supervised Temporal Sentiment Localization

Cailing Han^{1*} Zhangbin Li^{1*} Jinxing Zhou^{2†}
 Wei Qian¹ Jingjing Hu¹ Yanghao Zhou³ Zhangling Duan⁴ Dan Guo^{1,4,5†}
¹Hefei University of Technology ²MBZUAI ³NUS

⁴Institute of Artificial Intelligence, Hefei Comprehensive National Science Center

⁵The Key Laboratory of Knowledge Engineering with Big Data, Hefei University of Technology
 {ceilinghan, lizhangbin.mail, zhoujxhfut}@gmail.com, guodan@hfut.edu.cn

Abstract

Point-level weakly-supervised temporal sentiment localization (P-WTSL) aims to detect sentiment-relevant segments in untrimmed multimodal videos using timestamp sentiment annotations, which greatly reduces the costly frame-level labeling. To further tackle the challenges of imprecise sentiment boundaries in P-WTSL, we propose the Face-guided Sentiment Boundary Enhancement Network (FSENet), a unified framework that leverages fine-grained facial features to guide sentiment localization. Specifically, our approach first introduces the Face-guided Sentiment Discovery (FSD) module, which integrates facial features into multimodal interaction via dual-branch modeling for effective sentiment stimuli clues; We then propose the Point-aware Sentiment Semantics Contrast (PSSC) strategy to discriminate sentiment semantics of candidate points (frame-level) near annotation points via contrastive learning, thereby enhancing the model’s ability to recognize sentiment boundaries. At last, we design the Boundary-aware Sentiment Pseudo-label Generation (BSPG) approach to convert sparse point annotations into temporally smooth supervisory pseudo-labels. Extensive experiments and visualizations on the benchmark demonstrate the effectiveness of our framework, achieving state-of-the-art performance under full supervision, video-level, and point-level weak supervision, thereby showcasing the strong generalization ability of our FSENet across different annotation settings. Code: <https://github.com/CeilingHan/FSENet>.

1. Introduction

Driven by recent advances in audio-visual learning [1–20], Temporal Sentiment Localization (TSL), which aims to an-

*Equal contribution.

†Corresponding author.

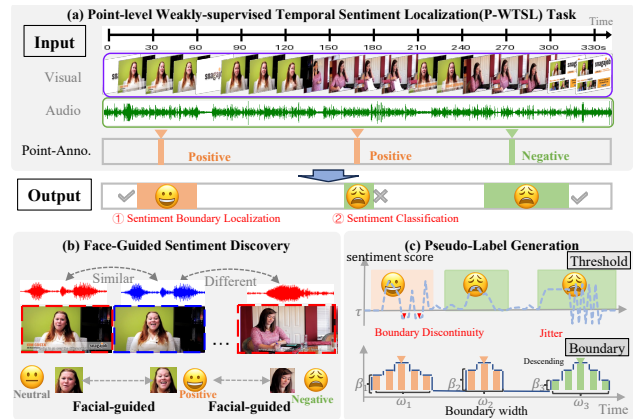


Figure 1. **Illustration of the task and motivation.** (a) Given the point-level sentiment points in the untrimmed video, the model needs to achieve sentiment classification and boundary localization. (b) We explored the facial-centric method to guide sentiment clues discovery. (c) To alleviate sentiment boundary jitter and discontinuity under weak supervision, we propose a novel pseudo-label smoothing strategy.

alyze sentiment in untrimmed audible videos, has become increasingly important for applications such as sentiment-adaptive editing [21, 22] and affect-aware summarization [23, 24]. However, acquiring dense frame-level sentiment annotations is time-consuming and costly, restricting the development of fully-supervised TSL [25–29]. As a result, the weakly-supervised temporal sentiment localization (WTSL) is receiving more and more attention from the community. Recent advances in WTSL mainly fall into two categories: (1) *video-level weakly-supervision*, where only entire video sentiment labels are available. DCIN [30] uses aligned subtitles as weak supervision via cross-modal consensus learning. Other weakly supervised methods include multiple instance learning [31, 32], reweighting-based mechanisms [33–36], and proposal scoring approaches [37,

38]. However, lacking fine-grained temporal labels, these methods often fail to precisely localize temporal boundaries. (2) *point-level weakly-supervision*, which uses a single point annotation per segment with the sentiment boundaries unknown. Recent models TSL [39] exploit temporal context and semantic alignment to infer sentiment segment localization.

In this research, we focus on point-level weakly-supervised TSL for videos, where the model aims to automatically locate fine-grained sentiment segments and classify their sentiment categories. As shown in Fig. 1(a), it constructs a mapping from sparsely annotated sentiment points and audio-visual modalities to segment-level sentiment boundary localization. However, this task has some core challenges: **1) Redundant Information Masks Salient Sentiment Signals.** Videos contain diverse visual and audio content, but key sentiment-related information is often obscured by redundant content (*e.g.*, ‘background’ or ‘color’), making it difficult for the model to mine effective sentiment information. **2) Uncertain Sentiment Boundaries Due to Sparse Point Annotations.** Point-level annotations in P-WTSL provide only a few sentiment anchors, making it difficult to determine precise sentiment boundaries. **3) Abrupt and Transient Sentiment Changes.** In realistic scenarios, sentiment may emerge and vanish abruptly within short temporal spans, which leads to significant challenges for accurate classification.

To address the above issues, we *first* propose to enhance video temporal sentiment localization using the **Facial Features**, for the three reasons: ① Facial expressions directly reflect sentiment stimuli [40, 41] in real scenarios; ② Subtle changes in the face area are easier to capture with lower difficulty, as shown in Fig. 1(b), whereas the overall temporal differences in the main visual content, such as ‘characters’ and ‘background’, are more difficult to perceive due to redundancy. ③ Face features are directly derived from visual frames and can better synergize learning with video features. To this end, to effectively leverage facial features for temporal sentiment localization, we propose the Face-Guided Sentiment Boundary Enhancement Network (FSENet). Specifically, a face-centric interaction module is designed, consisting of two stages: the facial features first interact independently with audio and visual. These relatively clean and unimodal features make it easier to detect sentiment cues. To further capture more complex sentiment, the fused representations Face-Audio ($F_a^{(f)}$) and Face-Visual ($F_v^{(f)}$) are employed to interact for sentiment expression. In parallel with the Facial-Centric Interaction branch, we incorporate a global sentiment perception weighting mechanism, which identifies potential sentiment-relevant segments from a holistic view. These two branches collaboratively leverage facial features to discover sentiment-stimulation cues for localization.

Importantly, the point-level supervised TSL task still faces two key challenges: vague sentiment boundaries and poor segment-level classification after the stimulus cues are found. Therefore, we further propose **two key optimization modules** to enhance sentiment semantic alignment. The Point-aware Sentiment Semantics Contrast (PSSC) (shown in Fig. 2(b)) performs frame-level sentiment semantics contrastive training on the temporal axis. Specifically, for each sentiment category (*e.g.*, positive), we aggregate annotated positive point features into a class-specific prototype. The top- k frames most similar to the class-specific prototype are selected as positives (\mathcal{U}^+), while other unannotated frames serve as negatives (\mathcal{U}^-). This contrastive training pulls positive frames closer in semantic space to improve segment sentiment classification. Moreover, the proposed Boundary-aware Sentiment Pseudo-label Generation (BSPG) module aims to produce high-quality pseudo-labels for reliable sentiment boundary modeling under point-level supervision. As illustrated in Fig. 1(c), traditional threshold-based methods [42] on frame-wise sentiment scores often suffer from *boundary discontinuity* and *jitter* due to score sensitivity and frame-level content noise, even after normalization. To address this, BSPG introduces a label smoothing mechanism that gradually decays sentiment scores from each annotation point using a decay factor β , with boundary width w controlling the extent of adjacent frames. This yields smoother, more coherent pseudo-labels, which are beneficial for determining effective sentiment boundaries. Our main contributions are as follows.:

- **Facial-Guided Multimodal Interaction for Sentiment Discovery.** We leverage facial features as key sentiment cues to guide audio-visual interaction, enabling interaction and global branches to discover more accurate sentiment cues amid complex background content.
- **Sentiment boundary optimization under weakly-supervised.** We design a contrastive scheme that pulls sentiment-consistent frames toward class prototypes derived from point annotations to enhance sentiment semantics consistency, and generate smoothing pseudo-labels by expanding annotation points into the temporal axis to improve boundary continuity and reduce noise.
- **Unified framework with strong generalization.** Our method provides a unified solution achieving state-of-the-art performance under full supervision and video-/point-level weak supervision, demonstrating strong generalization across varying settings, even with LLM methods.

2. Related Work

2.1. Multimodal Sentiment Analysis

Multimodal Sentiment Analysis (MSA) leverages visual, audio, and textual information to predict emotion for cropped videos [26]. Some approaches [43–46] decom-

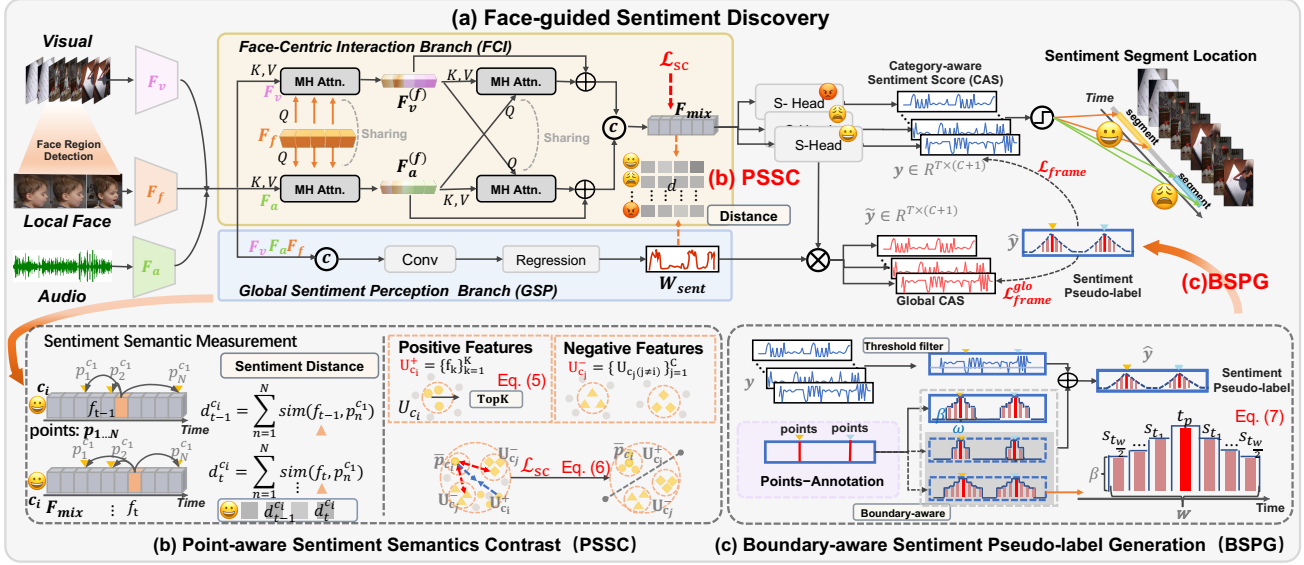


Figure 2. Overview of our FSENet framework. (a)FSD module introduces *facial features* into the temporal sentiment localization task through two branches to advance discovery of sentiment clues: *one* focuses on facial-centric interaction, while *the other* employs global sentiment perception weighting score. (b)PSSC aims to identify similar and dissimilar semantic *points* in the temporal axis to enhance the *point-level sentiment discrimination* by contrastive learning. (c)BSPG transforms *sentiment point-level annotations* into *segment-level sentiment boundaries pseudo-label* using the threshold filtering and step-by-step boundary-aware scheme, where sentiment scores decay progressively based on parameters β and w .

pose features into shared and modality-specific subspaces to help capture consistent emotions across multimodal information. Some work focus on the modality imbalance, filtering out noise from single modalities before fusion [47, 48] and removing noise from irrelevant frames to achieve better emotion recognition [49]. In addition, some work attempt to re-modify the prompt text to support the classification of emotion category [50, 51]. However, current MSA methods are still limited to coarse classification of pre-cropped video clips and are incapable of handling untrimmed videos [52]. Our framework advances toward fine-grained multi-emotion understanding and temporal boundary localization in untrimmed videos.

2.2. Temporal Boundary Localization

Temporal boundary localization aims to detect the occurrence time of events in untrimmed videos. Common methods [53–56] first generate a Class Activation Sequence and then apply a fixed threshold for boundary detection. However, these baseline approaches are primarily designed to learn better action representations for locating action boundaries, making them incapable of handling the subtle and dynamic nature of sentiment cues (e.g., facial expressions). Recent Temporal Sentiment Localization studies [39] use point supervision to jointly classify and localize sentiment segments, typically via inverse mapping and contrastive learning. However, they overlook temporal cross-

modal dependencies(e.g., synchrony between facial expressions, visuals, and audio) and sentiment semantic opposition (e.g., positive vs. negative sentiment). In contrast, our method leverages facial emotion guidance to enhance cross-modal consistency and contrast between sentiment semantics, thereby significantly improving localization accuracy.

3. Methodology

3.1. Problem Formulation

Given an sentiment audible video with T frames, the point-level annotations along timeline are provided as $Y_{\text{anno}} = \{(t_i, y_{t_i})\}_{i=1}^N$, where i -th point is denoted as p_i , and $p_i \in \mathbb{R}^C$ is a one-hot vector which notes the sentiment categories. The point-level weakly-supervised temporal sentiment localization (P-WTSL) task aims to predict segments conveying sentiment around annotated points.

3.2. Face-guided Sentiment Discovery (FSD)

To effectively incorporate facial cues into temporal sentiment localization, we propose the Face-guided Sentiment Discovery(FSD) main module, which integrates facial cues to guide and enhance interaction with audio/visual modalities for sentiment temporal alignment. FSD is designed with two parallel branches, Face-Centric Interaction (FCI) and Global Sentiment Perception (GSP) branches. They cooperate with each other to assist in the discovery of sentiment.

Face-Centric Interaction (FCI) leverages facial embeddings as semantic guidance to selectively attend to emotionally salient segments, shown in Fig. 2(a). Prior approaches [30, 39] generally overlook the role of facial features in TSL, but our strategy leverages facial embeddings to guide audio/visual feature interaction and highlight sentiment-relevant temporal segments. Specifically, given facial feature F_f , visual feature F_v , and auditory feature F_a , where $F_f, F_a, F_v \in \mathbb{R}^{T \times d}$, the first stage face-guided interaction is formulated as follows:

$$\begin{aligned} F_v^{(f)} &= F_v + \text{MHAttn}(F_f, F_v, F_v), \\ F_a^{(f)} &= F_a + \text{MHAttn}(F_f, F_a, F_a), \end{aligned} \quad (1)$$

where the $\text{MHAttn}(\cdot)$ denotes the multi-head attention [57], with its inputs corresponding to the ‘query’, ‘key’, and ‘value’, respectively. The outputs $F_v^{(f)}, F_a^{(f)} \in \mathbb{R}^{T \times d}$ are face-guided fusion features in stage-I.

To further enable comprehensive sentiment clues discovery, we design the stage-II face-guided interaction to progressively integrate audio and visual features with the impact of facial features, which performs deep multimodal interaction. The process is formulated as follows:

$$\begin{aligned} F_v^{(af)} &= F_v^{(f)} + \text{MHAttn}(F_a^{(f)}, F_v^{(f)}, F_v^{(f)}), \\ F_a^{(vf)} &= F_a^{(f)} + \text{MHAttn}(F_v^{(f)}, F_a^{(f)}, F_a^{(f)}), \end{aligned} \quad (2)$$

where the fusion output $F_v^{(af)}$ and $F_a^{(vf)} \in \mathbb{R}^{T \times d}$. We concatenate them to obtain the fused representation $F_{\text{mix}} = [F_v^{(af)}; F_a^{(vf)}] \in \mathbb{R}^{T \times 2d}$.

Global Sentiment Perception (GSP) weighting strategy is designed to complement the interaction branch by modeling sentiment intensity. While the Face-Centric Interaction branch enhances temporal alignment across modalities through facial feature guided interactions, this global branch takes a holistic view, identifying sentimentally salient segments along frame-level emotional stimulation dependencies. Specifically, modality-specific features F_a, F_v , and F_f are first concatenated, then fed into the convolutional layers $E(\cdot)$. Then the output is projected by regression head $\text{Reg}(\cdot)$ with a sigmoid activation $\sigma(\cdot)$ to produce the sentiment weight $W_{\text{sent}} \in \mathbb{R}^{T \times 1}$, and weighting $W_{\text{sent}} \in [0, 1]$:

$$W_{\text{sent}} = \sigma(\text{Reg}(E([F_a; F_v; F_f]))) \quad (3)$$

3.3. Point-aware Sentiment Semantics Contrast (PSSC)

To enhance the boundary localization of sentiment semantics around annotation points under weak supervision, we propose the PSSC optimization strategy, as illustrated Fig. 2(b). The capability of this strategy is to leverage point-level sentiment annotations to pull temporally points (at the

frame-level) with the same sentiment closer in the embedding space. Specifically, for each candidate point embedding f_t on the temporal axis, we measure its distance to all annotated points $p_{1 \dots n}^{c_i}$. The computation is performed as follows:

$$d_t^{c_i} = \sum_{n=1}^N \text{sim}(f_t, p_n^{c_i}), \quad (4)$$

where $\text{sim}(\cdot, \cdot)$ denotes the feature similarity (*i.e.*, cosine similarity), and value $d \in [0, 1]$, and the number N means the annotated points of sentiment of c_i .

Next, we construct positive and negative sample sets for contrastive learning, based on the computed distances. To gain sentiment stimulation, we incorporate Global Sentiment Perception weighting (GSP) in Eq. 3, which can adjust sample selection based on sentiment saliency. The positive neighbor set for category c_i , denoted as \mathcal{U}_{c_i} , consists of the top- K most relevant point embeddings:

$$\mathcal{U}_{c_i}^+ = \{f_t \mid d_t^{c_i} \in \text{Top-}K(\{W_{\text{sent},t} \cdot d_t^{c_i}\}_{t=1}^T)\}, \quad (5)$$

where $K < T - N$ is a parameter controlling the size of the positive set $\mathcal{U}_{c_i}^+$, which consists of point-level embeddings, and $t \neq t_p$ (t_p : annotated timestamp). Meanwhile, for other sentiment categories $c_j \neq c_i$, nearby points form negative sets $\mathcal{U}_{c_j}^-$, as they belong to different sentiment prototypes.

To enhance the discriminative ability for sentiment classification under point-level supervision, we introduce a contrastive learning loss to encourage candidate points to be close to their annotation points with the same sentiment category, while simultaneously pushing them away from neighbors of different categories. To this end, we construct a triplet $\{\bar{p}_{c_i}, \mathcal{U}_{c_i}^+, \mathcal{U}_{c_j}^-\}$ for sentiment c_i . The \bar{p}_{c_i} serves as a sentiment prototype, encouraging features in the positive set $\mathcal{U}_{c_i}^+$ to be pulled closer to \bar{p}_{c_i} , while pushing features in the negative sets $\mathcal{U}_{c_j}^-$ away. The overall loss across all sentiment categories is defined as:

$$\mathcal{L}_{\text{sc}} = - \sum_{i=1}^C \log \frac{\sum_{f_t \in \mathcal{U}_{c_i}^+} \exp(f_t \cdot \bar{p}_{c_i})}{\sum_{f_t \in \{\mathcal{U}_{c_i}^+, \mathcal{U}_{c_j}^-\}} \exp(f_t \cdot \bar{p}_{c_{k=i/j}})}, \quad (6)$$

where \bar{p}_{c_i} is the average result of the annotation point features for sentiment category c_i , and k in negative sets is based on the sentiment to which f_t belongs.

3.4. Boundary-aware Sentiment Pseudo-label Generation (BSPG)

The quality of the generated pseudo-label \hat{y} , especially the accuracy of its sentiment boundaries, plays a pivotal role in the effectiveness of the point-level WTSL task. To address the challenge of jitter and discontinuous pseudo-label distributions caused by using raw model predictions with a threshold filter [42, 58]. We propose a *Boundary-aware Sentiment Pseudo-label Generation* (BSPG) strategy that exploits the local temporal continuity of sentiment frames

near annotation points. The detailed procedure is as follows:

$$\mathbf{s}_t = \beta + (1 - \beta) \left(1 - \frac{|t - t_p|}{w}\right), \quad (7)$$

where t_p is the timestamp of the annotated point, and t is any time step along the video, and $w \in \mathbb{Z}^+$ and $\beta \in [0, 1]$ are the predefined hyperparameters denoting the smoothing window length (frames-level) and smoothing score that controls the minimum pseudo-label value at the temporal boundaries, respectively.

Next, we integrate the output sentiment score \mathbf{y} and the obtained smoothing scores \mathbf{s}_t to enhance the reliability of sentiment localization supervision:

$$\hat{\mathbf{y}}_{t,c_i} = \mathbb{I}(\mathbf{y}_t) + \begin{cases} \mathbf{s}_t, & \text{if } c_i \neq c+1 \text{ and } |t - t_p| \leq w, \\ 1 - \mathbf{s}_t, & \text{if } c_i = c+1 \text{ and } |t - t_p| \leq w, \\ 0, & \text{otherwise,} \end{cases} \quad (8)$$

where $c_i = c+1$ represents the non-sentiment category, and $\mathbb{I}(\mathbf{y}_t)$ denotes a sentiment threshold function that sets the sentiment score to zero when non-sentiment confidence \mathbf{y}_t exceeds threshold $\tau=0.95$, indicating a non-sentiment point.

3.5. Optimization of Backbone Network

To adapt the point-level weakly supervised temporal sentiment localization, we leverage the previously obtained F_{mix} and W_{sent} features to construct an effective loss function for optimizing our framework. Specifically, the F_{mix} is processed through $c+1$ independent convolutional layers with a sigmoid-activated function to generate the frame-level sentiment score for sentiment alignment supervision, and the process is as follows:

$$\mathbf{y} = \sigma(\text{CLS}(F_{\text{mix}})) \in \mathbb{R}^{T \times (C+1)}, \quad (9)$$

where the number C denotes sentiment categories, with an additional category designated for non-sentiment. The output \mathbf{y} denotes the frame-level category-aware sentiment score (CAS).

Next, we further achieve feature-level collaboration between the two branches, incorporating the category-aware sentiment score (CAS) into the global sentiment perception (GSP) branch for joint computation:

$$\tilde{\mathbf{y}}_t = [W_{\text{sent},t} \cdot \mathbf{y}_{t,1:C}; (1 - W_{\text{sent},t}) \cdot \mathbf{y}_{t,C+1}], \quad (10)$$

where the larger value in W_{sent} reflect stronger sentiment stimuli in the first c categories, meanwhile $1 - W_{\text{sent}}$ is used to represent the last non-sentiment category, and $\tilde{\mathbf{y}}_t \in \mathbb{R}^{C+1}$ is the sentiment-enhanced activation for frame t , and $\tilde{\mathbf{y}} \in \mathbb{R}^{T \times (C+1)}$ denotes the (Global CAS) in global branch.

Our optimization objective is to minimize the discrepancy between the category-aware sentiment score (CAS) and the global CAS with the sentiment pseudo label $\hat{\mathbf{y}}$ generated from point-level annotations. To guide the training

process, we define a base loss $\mathcal{L}_{\text{base}} = -\sum_{c=1}^C \text{avg}(\hat{\mathbf{y}}_c) \cdot \log \text{avg}(\mathbf{y}_c)$ that encourages alignment of (video-level) sentiment predictions by averaging over temporal axis. We also introduce two finer-grained (frame-level) supervision constraints, $\mathcal{L}_{\text{frame}}$ and $\mathcal{L}_{\text{frame}}^{\text{glo}}$, whose details are as follows:

$$\begin{aligned} \mathcal{F}_{\text{align}}(\mathbf{f}; \mathbf{f}_p) &= \sum_{c=1}^{C+1} \text{FL}(\mathbf{f}; \mathbf{f}_p), \\ \mathcal{L}_{\text{frame}} &= \mathcal{F}_{\text{align}}(\mathbf{y}; \hat{\mathbf{y}}); \quad \mathcal{L}_{\text{frame}}^{\text{glo}} = \mathcal{F}_{\text{align}}(\tilde{\mathbf{y}}; \hat{\mathbf{y}}), \end{aligned} \quad (11)$$

$\mathbf{y} \leftarrow \text{FCI} \quad \tilde{\mathbf{y}} \leftarrow \text{GSP} \quad \hat{\mathbf{y}} \leftarrow \text{BSPG}$

where the $\mathcal{F}_{\text{align}}(\cdot; \cdot)$ function performs **Frame-level Sentiment Alignment** between the model outputs (\mathbf{y} and $\tilde{\mathbf{y}}$) and the pseudo labels ($\hat{\mathbf{y}}$). The FL denotes the focal loss function [59] with γ is 2, which is widely used in multimodal sentiment analysis tasks to help distinguish sentiment-related frames from non-sentiment ones.

In summary, the overall backbone network is trained on the point-level WTSL task with multiple loss functions. The collaborative loss computation $\mathcal{L}_{\text{total}}$ is as follows:

$$\mathcal{L}_{\text{total}} = \mathcal{L}_{\text{base}} + \lambda_1 \cdot (\mathcal{L}_{\text{frame}} + \mathcal{L}_{\text{frame}}^{\text{glo}}) + \lambda_2 \mathcal{L}_{\text{sc}}, \quad (12)$$

where the hyperparameters λ_1 and λ_2 are weighting factors that balance the relative importance of the respective terms in the total loss.

4. Experiments

4.1. Experimental Setup

Dataset and Evaluation Metrics. We primarily evaluate our method on the popular point-annotated TSL300 [39] dataset, which contains 300 untrimmed videos with an average duration of over 250 seconds, totaling more than 1.3k minutes. We also evaluate our method on CMU-MOSEI [64], where we retain two sentiment categories for temporal localization on untrimmed videos. Following the standard protocol [39], we use mean Average Precision (mAP) under IoU thresholds from 0.1 to 0.3 (step size 0.05) as the primary metric for temporal localization. Additionally, we report Recall and F2-score metrics to better evaluate segment-level sentiment classification.

Implementation Details. Videos are divided into 16-frame segments to extract visual, audio, and facial features using the I3D [65], MFCC [66], and ResEmoteNet [67], respectively. Facial regions are detected using DeepFace¹ to obtain bounding boxes: [x,y,w,h], which are then fed into ResEmoteNet for feature extraction. The raw feature dimensions (1024/512/256) are projected to a unified dimension $d=512$ via unfixed 1D convolutions. We use the Adam optimizer, with an initial learning rate of 1×10^{-5} and a weight decay of 5×10^{-4} . The training epochs are 600, and

¹<https://github.com/serengil/deepface>

Table 1. **Performance comparison with SOTA methods under Fully and Weakly supervised settings on TSL300.** “†” indicates methods reproduced by ourselves. The best and second-best results are **bolded** and underlined, respectively.

Setting	Method	mAP@IoU(%)					Average		
		0.1	0.15	0.2	0.25	0.3	Recall	F2 Score	mAP
Full Supervision	VAANet [60]	28.01	24.95	20.68	16.45	<u>12.50</u>	69.82	39.59	20.51
	†AFSD [61]	33.44	27.09	<u>21.78</u>	<u>16.64</u>	11.76	<u>75.10</u>	<u>31.78</u>	22.14
	FSENet(ours)	<u>28.02</u>	<u>25.45</u>	22.63	18.93	14.33	79.58	30.37	<u>21.87</u>
Weak Supervision (Video-level)	CoLA [62]	11.87	10.14	8.11	6.83	4.98	<u>64.07</u>	21.19	8.38
	UM [34]	14.77	<u>13.28</u>	<u>10.77</u>	8.41	6.54	55.33	23.94	<u>10.75</u>
	†DDG-Net [54]	<u>16.13</u>	12.19	9.91	<u>8.47</u>	<u>6.93</u>	66.38	23.82	10.72
	†ISSF [55]	13.83	11.15	9.30	6.87	5.14	45.65	25.17	9.26
	†TSL [39]	14.10	11.35	8.77	6.36	4.47	31.84	<u>27.40</u>	9.01
	FSENet(ours)	19.15	15.12	11.91	9.35	7.12	58.11	30.0	12.53
Weak Supervision (Point-level)	LACP [42]	17.25	14.46	12.47	9.59	7.76	66.92	25.01	12.30
	SF-Net [63]	20.26	18.09	15.01	12.38	9.76	59.55	32.61	15.10
	†HR-pro ^{stage1} [56]	19.77	17.10	14.71	11.38	8.86	62.23	22.82	14.36
	†HR-pro ^{stage2} [56]	27.24	23.13	19.85	15.96	<u>11.83</u>	<u>73.60</u>	32.21	19.60
	TSL [39]	<u>28.72</u>	<u>24.92</u>	<u>20.46</u>	<u>16.10</u>	<u>11.83</u>	71.14	35.36	<u>20.40</u>
	FSENet(ours)	29.31	25.47	22.49	16.76	13.24	75.02	<u>33.67</u>	21.45

Table 2. **Performance results on CMU-MOSEI dataset** under point-level settings.

Method	mAP@IoU(%)			Average		
	0.1	0.2	0.3	Recall	F2 Score	mAP
HR-pro ^{stage1}	11.83	7.26	4.44	18.81	18.46	7.65
HR-pro ^{stage2}	16.27	11.49	6.76	26.61	24.71	11.47
TSL	15.18	10.71	7.46	27.24	24.86	11.00
FSENet (Ours)	22.7	22.49	13.24	33.08	24.89	16.54

Table 3. **Comparison with large language models (LLMs)** on the TSL300 dataset. Zero-shot methods are evaluated without fine-tuning, while LoRA-based models are fine-tuned with point-level supervision.

Method	mAP@IoU (%)			Avg mAP
	0.1	0.2	0.3	
Qwen3-Omni(zero-shot)	7.67	5.03	2.67	5.07
LLaMA-2-7B (LoRA)	10.98	10.98	8.45	9.97
LLaMA-2-7B (LoRA+BSPG)	27.76	11.82	5.16	11.75
Ours (small model)	29.31	22.49	13.24	21.45

the batch size is 16. The experiments are conducted on a single NVIDIA A40 GPU. The optimization of total losses contains two parameters: $\lambda_1=1$ and $\lambda_2=0.05$. The hyper-parameters $w=7$ and $\beta=0.6$ are applied in Eq. 7 and Eq. 8, respectively. **Supervision settings:** We compare point-level, video-level weak, and full supervision settings for TSL. For weak supervision, only point annotations are used. For the video-level setting, points are converted into a binary vector \mathbb{R}^C , where 1 indicates the presence of sentiment segments. For full supervision, segment start and end times are converted into frame-level labels.

Table 4. **Fair evaluation under identical feature settings on TSL300.** Group ① uses only audio-visual features, and group ② adds local facial features. All Δ adopt the same facial extractor.

Method	mAP@IoU (%)					Avg mAP
	0.1	0.15	0.2	0.25	0.3	
<i>AV Features Only</i>						
HR-pro ^{stage1}	16.64	13.95	11.86	9.74	8.01	12.04
HR-pro ^{stage2}	26.40	21.80	16.91	13.27	9.96	17.67
TSL	28.14	23.02	18.68	14.36	10.46	18.93
FSENet(ours)	25.91	24.70	20.08	16.85	11.53	19.41
<i>AV + Facial Features</i>						
Δ HR-pro ^{stage1}	19.77	17.10	14.71	11.38	8.86	14.36
Δ HR-pro ^{stage2}	27.24	23.13	19.85	15.96	11.83	19.60
Δ TSL	27.77	24.94	20.93	17.15	13.48	20.86
Δ FSENet(ours)	29.31	25.47	22.49	16.76	13.24	21.45

4.2. Comparison to Prior Work

We evaluate our model under multiple supervision settings, including full, video-level, and point-level supervision, to assess its effectiveness on the temporal sentiment localization task across the TSL300 and CMU-MOSEI datasets.

TSL300: As shown in Tab. 1, under point-level setting, our model achieves superior performance, attaining the best mAP scores across all IoU thresholds [0.1:0.3], and the highest average mAP@IoU of 21.45%, outperforming the previous SOTA method TSL [39] by over 5%, and achieving a peak Recall of 75.02%. Moreover, our model (FSENet) also demonstrates competitive results under both full and video-level weak supervision. First, our method surpasses the video-level supervised SOTA methods, such as UM [34], by 25% in F2-score and 16.5% in average mAP. Next, FSENet achieves a mAP of 21.87% and an F2-score of 30.37% under full supervision, approaching the perfor-

Table 5. Ablation study on the main network component in FSD. We report the result of mAPs, and ‘-’ denotes not used.

#id	FCI		GSP	mAP@IoU (%)			Avg mAP
	first stage	second stage		0.1	0.2	0.3	
a	-	-	✓	24.95	18.63	11.52	18.42
b	✓	-	✓	27.19	18.93	11.16	19.10
c	-	✓	✓	27.46	18.31	10.37	18.78
d	✓	✓	-	28.69	20.83	11.26	20.22
e	✓	✓	✓	29.31	22.49	13.24	21.45

Table 6. Ablation of pseudo-label generation strategies.

Pseudo-Label	Threshold	Boundary	mAP@IoU(%)			Avg mAP
			0.1	0.2	0.3	
None	-	-	27.51	15.31	8.72	16.92
Threshold Only	✓	-	28.06	20.98	11.55	20.29
Step Only	-	✓	25.76	21.59	13.10	20.31
Ours (full model)	✓	✓	29.31	22.49	13.24	21.45

mance of AFSD [61], which is specifically designed for the fully supervised setting. Our FSENet still surpasses this fully supervised method by around 6% in Recall.

CMU-MOSEI: To further verify generalization, we evaluate FSENet on the CMU-MOSEI dataset. In Tab. 2, FSENet achieves mAP@IoU thresholds of 22.7%, 22.49%, 13.24% for 0.1, 0.2, and 0.3, respectively. Despite the overall lower performance due to coarse temporal annotations, FSENet achieves 16.54% average mAP, outperforming TSL and HR-pro by 5.54% and 5.07%, respectively.

Comparison with LLMs. We compare our model with large language models (LLMs). Despite their strong reasoning ability, LLMs’ text-centric representations hinder temporal sentiment alignment across audio/visual/facial modalities. As shown in Tab. 3, our model achieves the highest average mAP of 21.45%, outperforming Qwen3-Omni-30B [68], LLaMA-2-7B [69] with LoRA [70], and LoRA + BSPG by 16.30%, 11.48%, and 9.70%, respectively. Moreover, for LLaMA-2 fine-tuning, our pseudo-labeling strategy BSPG (Eq. 8) improves average mAP by 1.8% over the variant without BSPG, demonstrating its effectiveness for temporal sentiment detection.

4.3. Ablation Studies

Ablation studies on facial features. To evaluate the impact of facial features, we conduct two group experiments: 1) using only audio-visual (AV) features, and 2) enhancing AV features with local facial features. As shown in Tab. 4, our method outperforms the SOTA method by 0.48% even without facial features. With facial feature enhancement, the performance of FSENet improves consistently across all IoU thresholds [0.1:0.3], reaching an average mAP of 21.45% and outperforming Δ TSL [39] by 0.59%. These results indicate that facial features improve sentiment localization, and FSENet achieves the best performance across all settings, confirming the generalizability of our design.

Table 7. Ablation of weakly-supervised optimization losses.

#id	$\mathcal{L}_{\text{frame}}$	$\mathcal{L}_{\text{frame}}^{\text{glo}}$	\mathcal{L}_{sc}	mAP@IoU(%)			Avg mAP
				0.1	0.2	0.3	
a	✓	✓	✓	29.31	22.49	13.24	21.45
b	-	✓	✓	28.28	19.52	10.33	20.02
c	✓	-	✓	27.67	20.40	9.99	20.65
d	✓	✓	-	29.17	21.18	12.49	20.94
e	-	-	✓	19.15	11.91	7.12	12.53
f	-	-	-	16.61	12.32	9.38	10.69

Effects of Main Network Components. The FSD framework consists of two parallel components: FCI and GSP. We conduct an ablation study to evaluate their contributions (Tab. 5). Compared to (row #a), (rows #b and #c) show slight improvements of 0.7% and 0.4%, respectively, when facial feature guidance is introduced into FCI. However, directly applying the complex second-stage fusion of $F_a^{(f)}$ and $F_v^{(f)}$ (Eq. 2 in (row #c) does not lead to obvious improvements. The best performance is achieved with an Avg.mAP of 21.45% (row #e), where facial guidance is progressively introduced (including both stages). Moreover, when the GSP branch is ablated (from row #e to #d), the performance drops by around 1.2%, highlighting the effectiveness of both the proposed FCI and GSP modules in leveraging facial features to enhance sentiment localization.

Effects of the generated pseudo-label. Our Boundary-aware Sentiment Pseudo-label Generation (BSPG) strategy combines a traditional threshold-based approach with a novel point-centric, step-wise boundary generation method (Tab. 6). The naive baseline using raw predictions suffers from low-confidence noise (16.92% mAP). Applying a confidence threshold improves the result to 20.29%, while our boundary-aware pseudo-label method refines temporal consistency and further boosts mAP to 20.31%. Our full approach (BSPG) achieves the best result (21.45% mAP) and improvement ($\approx 4.5\%$), demonstrating that our joint design effectively facilitates sentiment boundary localization under weak supervision.

Effects of the optimization. The losses $\mathcal{L}_{\text{frame}}$ and $\mathcal{L}_{\text{frame}}^{\text{glo}}$ (Eq. 11) enforce sentiment boundary constraints between the outputs of the two branches and the pseudo-labels under weak supervision. The semantic contrast loss \mathcal{L}_{sc} (Eq. 6) further aligns annotation points with nearby sentiment-relevant frames. We conduct an ablation study on these optimization losses, as shown in Tab. 7. Compared with the full optimization setting (row #a), removing each optimization loss (#b/#c/#d) leads to performance drops of around 1.4%, 0.8%, and 0.5%, respectively. Notably, jointly removing $\mathcal{L}_{\text{frame}}$ and $\mathcal{L}_{\text{frame}}^{\text{glo}}$ causes a significant drop of 8.9%, demonstrating the effectiveness of our pseudo-label design for sentiment boundary constraints. Overall, the results confirm that all proposed optimization losses contribute to improving temporal sentiment localization.

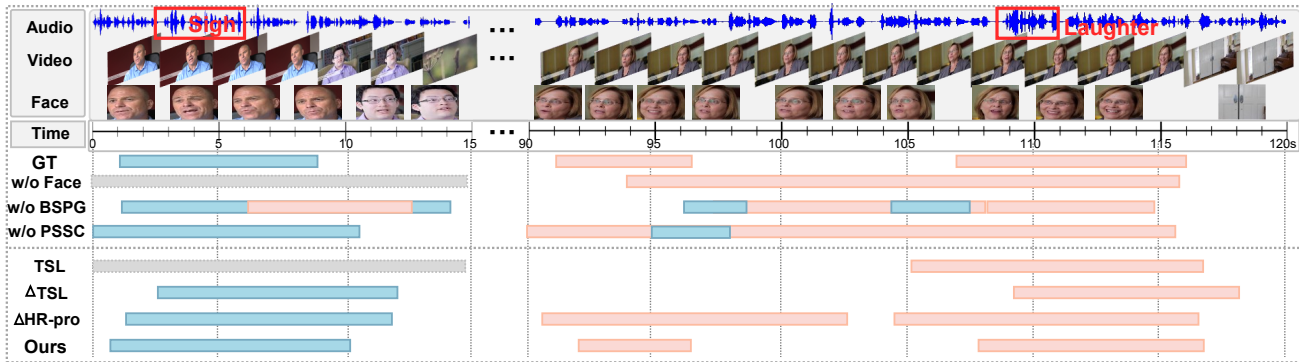


Figure 3. Visualization of the predicted results for temporal sentiment localization. The ‘pink’ segments are positive sentiment, ‘blue’ means negative, and ‘gray’ means no valid location output. Δ indicates that methods incorporate facial features settings.

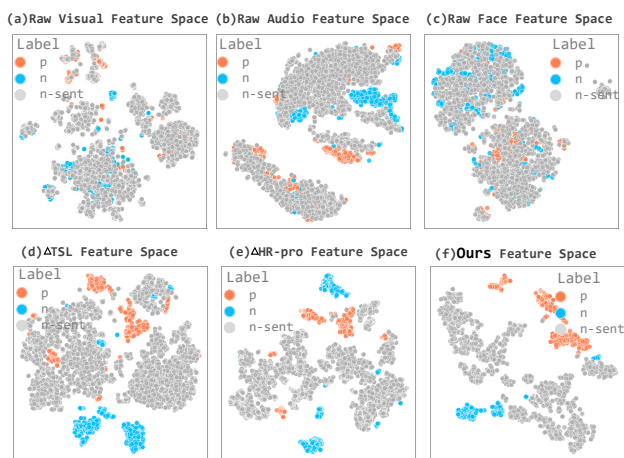


Figure 4. T-SNE visualization comparing our FSENet with SOTA. Each point represents a segment-level feature (‘p/n/n-sent’ denotes positive, negative, and non-sentiment categories, respectively).

4.4. Qualitative Results

Visualization of predicted sentiment localization. As illustrated in Fig. 3, we present a long-form interview discussing U.S. student loans, involving three speakers whose sentiments shift from initially negative to increasingly positive. The results are grouped for analysis. The *first* four outputs correspond to ablations of our main modules. Without facial features (w/o Face), the model fails to detect the early negative sentiment segment (0–15s) due to the lack of facial guidance. Removing our proposed optimization strategies (w/o BSPG and w/o PSSC) leads to fragmented sentiment predictions between (90–116s), indicating weaker temporal coherence and boundary precision. The latter four outputs compare our method with existing methods. TSL [39] and Δ TSL miss the fine-grained positive segment from (90–96s), suggesting limited sensitivity to short-duration sentiment shifts. Although Δ HR-pro [56] detects all emotional

segments, it tends to overextend short segments into overly long ones, leading to boundary overestimation. Our FSENet achieves the most accurate and balanced results, effectively capturing both short and long sentiment segments by leveraging facial cues and robust boundary strategies.

T-SNE visualization of the sentiment points distribution. To evaluate the effectiveness of our model in learning sentiment semantics, we randomly select four videos from TSL300 [39] and apply t-SNE to their frame-level features. Fig. 4(a)–(c) show the feature spaces of the original visual, audio, and facial features, where points with the same sentiment label are not clearly clustered. We then compare several state-of-the-art methods, including Δ TSL [39] and Δ HR-pro [56], as shown in Fig. 4(d)–(e). The t-SNE results show multiple sentiment clusters for both positive and negative samples, indicating a limited ability to distinguish sentiments. In contrast, our method, FSENet (Fig. 4(f)), produces two well-separated clusters corresponding to positive and negative sentiments with a large inter-cluster distance, facilitating more accurate temporal sentiment localization. This demonstrates the strong capability of our method in discriminating sentiment semantics.

5. Conclusion

In this paper, we propose FSENet, a unified framework for point-level weakly-supervised temporal sentiment localization (P-WTSL). We attempt to enhance sentiment stimuli discovery by introducing facial features as core semantic guidance (FSD), which facilitates interaction between audio/visual and facial features. Through facial-guided interaction, our model enhances sentiment boundary perception by jointly performing semantic contrastive learning (PSSC) and generating boundary-aware pseudo-labels (BSPG) that provide sentiment temporal supervision. Comprehensive experiments and ablation analyses confirm that FSENet achieves superior performance to existing SOTA approaches under every supervision setting for TSL tasks.

Acknowledgement: This work is supported by the National Key R&D Program of China (NO.2024YFB3311600), the Natural Science Foundation of China (62272144), the Anhui Provincial Natural Science Foundation (2408085J040), the Major Project of the Anhui Provincial Science and Technology Breakthrough Program (202423k09020001), and the Fundamental Research Funds for the Central Universities (JZ2024AHST0337).

References

- [1] J. Zhou, D. Guo, R. Guo, Y. Mao, J. Hu, Y. Zhong, X. Chang, and M. Wang, "Towards open-vocabulary audio-visual event localization," in *CVPR*, 2025, pp. 8362–8371. 1
- [2] P. Zhao, J. Zhou, Y. Zhao, D. Guo, and Y. Chen, "Multimodal class-aware semantic enhancement network for audio-visual video parsing," in *AAAI*, 2025, pp. 10 448–10 456.
- [3] Z. Li, D. Guo, J. Zhou, J. Zhang, and M. Wang, "Object-aware adaptive-positivity learning for audio-visual question answering," in *AAAI*, 2024, pp. 3306–3314.
- [4] Z. Li, J. Zhou, J. Zhang, S. Tang, K. Li, and D. Guo, "Patch-level sounding object tracking for audio-visual question answering," in *AAAI*, vol. 39, no. 5, 2025, pp. 5075–5083.
- [5] X. Liu, N. Xia, J. Zhou, Z. Li, and D. Guo, "Towards energy-efficient audio-visual classification via multimodal interactive spiking neural network," *ACM Transactions on Multimedia Computing, Communications, and Applications*, vol. 21, no. 5, pp. 144:1–144:24, 2025.
- [6] J. Zhou, X. Shen, J. Wang, J. Zhang, W. Sun, J. Zhang, S. Birchfield *et al.*, "Audio-visual segmentation with semantics," *IJCV*, vol. 133, no. 4, pp. 1644–1664, 2025.
- [7] J. Zhou, Z. Zhou, Y. Zhou, Y. Mao, Z. Duan, and D. Guo, "Clasp: Cross-modal salient anchor-based semantic propagation for weakly-supervised dense audio-visual event localization," in *AAAI*, 2026.
- [8] J. Zhou, L. Zheng, Y. Zhong, S. Hao, and M. Wang, "Positive sample propagation along the audio-visual event line," in *CVPR*, 2021, pp. 8436–8444.
- [9] J. Zhou, D. Guo, and M. Wang, "Contrastive positive sample propagation along the audio-visual event line," *IEEE Transactions on Pattern Analysis and Machine Intelligence*, vol. 45, no. 6, pp. 7239–7257, 2023.
- [10] J. Zhou, D. Guo, Y. Mao, Y. Zhong, X. Chang, and M. Wang, "Label-anticipated event disentanglement for audio-visual video parsing," in *ECCV*, 2024, pp. 35–51.
- [11] J. Zhou, D. Guo, Y. Zhong, and M. Wang, "Advancing weakly-supervised audio-visual video parsing via segment-wise pseudo labeling," *International Journal of Computer Vision*, vol. 132, no. 11, pp. 5308–5329, 2024.
- [12] J. Zhou, J. Wang, J. Zhang, W. Sun, J. Zhang, S. Birchfield, D. Guo, L. Kong, M. Wang, and Y. Zhong, "Audio-visual segmentation," in *ECCV*, 2022, pp. 386–403.
- [13] D. Jin, Y. Zhou, J. Zhou, J. Ma, R. Guo, and D. Guo, "Sim-token: A simple baseline for referring audio-visual segmentation," in *ICASSP*, 2026, pp. 1–5.
- [14] J. Zhou, Y. Zhou, M. Han, T. Wang, X. Chang, H. Cholakkal, and R. M. Anwer, "Think before you segment: An object-aware reasoning agent for referring audio-visual segmentation," in *AAAI*, 2026, pp. 1–19.
- [15] R. Guo, X. Ying, Y. Chen, D. Niu, G. Li, L. Qu, Y. Qi, J. Zhou, B. Xing, W. Yue *et al.*, "Audio-visual instance segmentation," in *CVPR*, 2025, pp. 13 550–13 560.
- [16] M. I. Kurpath, J. M. Kaithakkodan, J. Zhou, S. S. Mulla-pillay, M. Almansoori, N. Ahsan, B. Kalmakhanbet, S. Shikhar, R. Lalla, J. Lahoud *et al.*, "A benchmark and agentic framework for omni-modal reasoning and tool use in long videos," *arXiv preprint arXiv:2512.16978*, 2025.
- [17] X. Shen, D. Li, J. Zhou, Z. Qin, B. He, X. Han, A. Li, Y. Dai, L. Kong, M. Wang *et al.*, "Fine-grained audible video description," in *CVPR*, 2023, pp. 10 585–10 596.
- [18] Y. Mao, X. Shen, J. Zhang, Z. Qin, J. Zhou, M. Xiang, Y. Zhong, and Y. Dai, "Tavgbench: Benchmarking text to audible-video generation," in *ACM MM*, 2024, pp. 6607–6616.
- [19] J. Zhou, Y. Zhou, Y. Wang, Z. Han, J. Ma, H. Ding, R. M. Anwer, and H. Cholakkal, "Audit after segmentation: Reference-free mask quality assessment for language-referred audio-visual segmentation," *arXiv preprint arXiv:2602.03892*, 2026.
- [20] Y.-H. Zhou, H. Li, R. Lin, H. Huang, J. Zhou, C. Yuan, T. Lan, Z. Zhou, Y. Li, J. Xu *et al.*, "Mtagv-bench: A comprehensive benchmark for evaluating multi-talker dialogue-centric audio-video generation," *arXiv preprint arXiv:2602.00607*, 2026. 1
- [21] X. Ji, H. Zhou, K. Wang, W. Wu, C. C. Loy, X. Cao, and F. Xu, "Audio-driven emotional video portraits," in *CVPR*, 2021, pp. 14 080–14 089. 1
- [22] Y. Wang, S. Shen, and B. Y. Lim, "Reprompt: Automatic prompt editing to refine ai-generative art towards precise expressions," in *ACM CHI*, 2023, pp. 1–29. 1
- [23] E. Apostolidis, E. Adamantidou, A. I. Metsai, V. Mezaris, and I. Patras, "Video summarization using deep neural networks: A survey," *Proceedings of the IEEE*, vol. 109, no. 11, pp. 1838–1863, 2021. 1
- [24] A. Bertrand, R. Belloum, J. R. Eagan, and W. Maxwell, "How cognitive biases affect xai-assisted decision-making: A systematic review," in *AAAI*, 2022, pp. 78–91. 1
- [25] S. Poria, E. Cambria, D. Hazarika, N. Majumder, A. Zadeh, and L.-P. Morency, "Context-dependent sentiment analysis in user-generated videos," in *ACL*, 2017, pp. 873–883. 1
- [26] A. Z. P. P. L. S. P. E. C. L.-P. Morency, "Multimodal language analysis in the wild: CMU-MOSEI dataset and interpretable dynamic fusion," in *ACL*, 2018, pp. 2236–2246. 2
- [27] N. Majumder, D. Hazarika, A. Gelbukh, E. Cambria, and S. Poria, "Multimodal sentiment analysis using hierarchical fusion with context modeling," *Knowledge-based systems(KBS)*, vol. 161, pp. 124–133, 2018.
- [28] W. Yu, H. Xu, Z. Yuan, and J. Wu, "Learning modality-specific representations with self-supervised multi-task learning for multimodal sentiment analysis," in *AAAI*, 2021, pp. 10 790–10 797.

- [29] Y.-H. H. Tsai, S. Bai, P. P. Liang, J. Z. Kolter, L.-P. Morency, and R. Salakhutdinov, "Multimodal transformer for unaligned multimodal language sequences," in *ACL*, 2019, pp. 6477–6486. 1
- [30] J. Li, J. Xie, L. Zhu, L. Qian, S. Tang, W. Zhang, H. Shi, S. Zhang, L. Wei, Q. Tian *et al.*, "Dilated context integrated network with cross-modal consensus for temporal emotion localization in videos," in *ACM MM*, 2022, pp. 5083–5092. 1, 4
- [31] L. Wang, Y. Xiong, D. Lin, and L. Van Gool, "Untrimmed-nets for weakly supervised action recognition and detection," in *CVPR*, 2017, pp. 4325–4334. 1
- [32] P. Nguyen, T. Liu, G. Prasad, and B. Han, "Weakly supervised action localization by sparse temporal pooling network," in *CVPR*, 2018, pp. 6752–6761. 1
- [33] F. Hong, J. Feng, D. Xu, and Y. Shan, "Cross-modal consensus network for weakly supervised temporal action localization," in *ACM MM*, 2021, pp. 3932–3941. 1
- [34] P. Lee, J. Wang, Y. Lu, and H. Byun, "Weakly-supervised temporal action localization by uncertainty modeling," in *AAAI*, 2021, pp. 1854–1862. 6
- [35] J. Zhou, Z. Li, Y. Yu, Y. Zhou, R. Guo, G. Li, Y. Mao, M. Han, X. Chang, and M. Wang, "Mettle: Meta-token learning for memory-efficient audio-visual adaptation," *IEEE Transactions on Pattern Analysis and Machine Intelligence*, pp. 1–17, 2025.
- [36] Z. Zhou, J. Zhou, W. Qian, S. Tang, X. Chang, and D. Guo, "Dense audio-visual event localization under cross-modal consistency and multi-temporal granularity collaboration," in *AAAI*, vol. 39, no. 10, 2025, pp. 10905–10913. 1
- [37] H. Ren, W. Yang, T. Zhang, and Y. Zhang, "Proposal-based multiple instance learning for weakly-supervised temporal action localization," in *CVPR*, 2023, pp. 2394–2404. 1
- [38] Y. Hu, J. Fu, M. Chen, J. Gao, J. Dong, B. Fan, and H. Liu, "Learning proposal-aware re-ranking for weakly-supervised temporal action localization," *IEEE Transactions on Circuits and Systems for Video Technology (TCSVT)*, vol. 34, no. 1, pp. 207–220, 2023. 2
- [39] Z. Zhang and J. Yang, "Temporal sentiment localization: Listen and look in untrimmed videos," in *ACM MM*, 2022, pp. 199–208. 2, 3, 4, 5, 6, 7, 8
- [40] M. A. Sama, M. Shoura, A. Nestor, and J. S. Cant, "Attention and stimulus structure interact during ensemble encoding of facial expression," *Scientific Reports*, vol. 15, no. 1, p. 18632, 2025. 2
- [41] N. Alp, G. Lale, C. Saglam, and B. Sayim, "The effect of processing partial information in dynamic face perception," *Scientific Reports*, vol. 14, no. 1, p. 9794, 2024. 2
- [42] P. Lee and H. Byun, "Learning action completeness from points for weakly-supervised temporal action localization," in *CVPR*, 2021, pp. 13648–13657. 2, 4, 6
- [43] D. Hazarika, R. Zimmermann, and S. Poria, "Misa: Modality-invariant and-specific representations for multimodal sentiment analysis," in *ACM MM*, 2020, pp. 1122–1131. 2
- [44] P. He, J. Yu, C. Ge, Y. Yu, W. Xu, L. Wang, T. Liu, and Z. Kan, "Domain-separated bottleneck attention fusion framework for multimodal emotion recognition," *ACM Transactions on Multimedia Computing, Communications and Applications (TOMCCAP)*, vol. 21, no. 4, pp. 1–21, 2025.
- [45] J. Zhang, L. Zheng, M. Wang, and D. Guo, "Training a small emotional vision language model for visual art comprehension," in *ECCV*. Springer, 2024, pp. 397–413.
- [46] P. Song, D. Guo, X. Yang, S. Tang, and M. Wang, "Emotional video captioning with vision-based emotion interpretation network," *IEEE Transactions on Image Processing*, vol. 33, pp. 1122–1135, 2024. 2
- [47] Y. Zeng, S. Mai, W. Yan, and H. Hu, "Multimodal reaction: Information modulation for cross-modal representation learning," *IEEE Transactions on Multimedia (TMM)*, vol. 26, pp. 2178–2191, 2024. 3
- [48] H. Zhang, Y. Wang, G. Yin, K. Liu, Y. Liu, and T. Yu, "Learning language-guided adaptive hyper-modality representation for multimodal sentiment analysis," *arXiv preprint arXiv:2310.05804*, 2023. 3
- [49] Z. Zhang, L. Wang, and J. Yang, "Weakly supervised video emotion detection and prediction via cross-modal temporal erasing network," in *CVPR*, 2023, pp. 18888–18897. 3
- [50] J. Wei, G. Hu, X. Yang, A. T. Luu, and Y. Dong, "Learning facial expression and body gesture visual information for video emotion recognition," *Expert Systems with Applications*, vol. 237, p. 121419, 2024. 3
- [51] T. Chay-intr, Y. Chen, K. Viriyayudhakorn, and T. Theeramunkong, "Llavac: Fine-tuning llava as a multimodal sentiment classifier," *arXiv preprint arXiv:2502.02938*, 2025. 3
- [52] U. Singh, K. Abhishek, and H. K. Azad, "A survey of cutting-edge multimodal sentiment analysis," *ACM Computing Surveys (CSUR)*, vol. 56, no. 9, pp. 1–38, 2024. 3
- [53] Y. Li, W. Gan, K. Lu, D. Jiang, and R. Jain, "Aves: An audio-visual emotion stream dataset for temporal emotion detection," *IEEE Transactions on Affective Computing (IEEE Trans. Affective Comput)*, vol. 16, no. 1, pp. 438–450, 2025. 3
- [54] X. Tang, J. Fan, C. Luo, Z. Zhang, M. Zhang, and Z. Yang, "Ddg-net: Discriminability-driven graph network for weakly-supervised temporal action localization," in *ICCV*, 2023, pp. 6622–6632. 6
- [55] W. Yun, M. Qi, C. Wang, and H. Ma, "Weakly-supervised temporal action localization by inferring salient snippet-feature," in *AAAI*, 2024, pp. 6908–6916. 6
- [56] H. Zhang, X. Wang, X. Xu, Z. Qing, C. Gao, and N. Sang, "Hr-pro: Point-supervised temporal action localization via hierarchical reliability propagation," in *AAAI*, 2024, pp. 7115–7123. 3, 6, 8
- [57] A. Vaswani, N. Shazeer, N. Parmar, J. Uszkoreit, L. Jones, A. N. Gomez, Ł. Kaiser, and I. Polosukhin, "Attention is all you need," *Advances in neural information processing systems*, vol. 30, 2017. 4
- [58] K. K. Rachavarapu, K. Ramakrishnan *et al.*, "Weakly-supervised audio-visual video parsing with prototype-based pseudo-labeling," in *CVPR*, 2024, pp. 18952–18962. 4
- [59] T.-Y. Lin, P. Goyal, R. Girshick, K. He, and P. Dollár, "Focal loss for dense object detection," in *ICCV*, 2017, pp. 2980–2988. 5

- [60] S. Zhao, Y. Ma, Y. Gu, J. Yang, T. Xing, P. Xu, R. Hu, H. Chai, and K. Keutzer, "An end-to-end visual-audio attention network for emotion recognition in user-generated videos," in *AAAI*, 2020, pp. 303–311. [6](#)
- [61] C. Lin, C. Xu, D. Luo, Y. Wang, Y. Tai, C. Wang, J. Li, F. Huang, and Y. Fu, "Learning salient boundary feature for anchor-free temporal action localization," in *CVPR*, 2021, pp. 3320–3329. [6](#), [7](#)
- [62] C. Zhang, M. Cao, D. Yang, J. Chen, and Y. Zou, "Cola: Weakly-supervised temporal action localization with snippet contrastive learning," in *CVPR*, 2021, pp. 16 010–16 019. [6](#)
- [63] F. Ma, L. Zhu, Y. Yang, S. Zha, G. Kundu, M. Feiszli, and Z. Shou, "Sf-net: Single-frame supervision for temporal action localization," in *ECCV*, 2020, pp. 420–437. [6](#)
- [64] A. Zadeh, P. P. Liang, S. Poria, P. Vij, E. Cambria, and L.-P. Morency, "Multimodal language analysis in the wild: Cmu-mosei dataset and interpretable dynamic fusion graph," in *ACL*, 2018, pp. 2236–2246. [5](#)
- [65] J. Carreira and A. Zisserman, "Quo vadis, action recognition? a new model and the kinetics dataset," in *CVPR*, 2017, pp. 6299–6308. [5](#)
- [66] L. Muda, M. Begam, and I. Elamvazuthi, "Voice recognition algorithms using mel frequency cepstral coefficient (mfcc) and dynamic time warping (dtw) techniques," *arXiv preprint arXiv:1003.4083*, 2010. [5](#)
- [67] A. K. Roy, H. K. Kathania, A. Sharma, A. Dey, and M. S. A. Ansari, "Resemotenet: bridging accuracy and loss reduction in facial emotion recognition," *IEEE Signal Processing Letters*, 2024. [5](#)
- [68] J. Xu, Z. Guo, H. Hu, Y. Chu, X. Wang, J. He, Y. Wang *et al.*, "Qwen3-omni technical report," *arXiv preprint arXiv:2509.17765*, 2025. [7](#)
- [69] H. Touvron, L. Martin, K. Stone, P. Albert, A. Almahairi, Y. Babaei, N. Bashlykov, S. Batra, P. Bhargava, S. Bhosale *et al.*, "Llama 2: Open foundation and fine-tuned chat models," *arXiv preprint arXiv:2307.09288*, 2023. [7](#)
- [70] E. J. Hu, Y. Shen, P. Wallis, Z. Allen-Zhu, Y. Li, S. Wang, L. Wang, and W. Chen, "Lora: Low-rank adaptation of large language models," in *International Conference on Learning Representations (ICLR)*, 2022. [7](#)
- [71] H. Alwassel, F. C. Heilbron, V. Escorcía, and B. Ghanem, "Diagnosing error in temporal action detectors," in *ECCV*, 2018, pp. 256–272. [1](#)

Face-Guided Sentiment Boundary Enhancement for Weakly-Supervised Temporal Sentiment Localization

Supplementary Material

Table 8. Ablation study of BSPG parameters (confidence decay factor β and smoothing width w) on mAP performance.

BSPG	w	5	6	7	8	9
	mAP (%)	19.22	19.77	21.45	19.66	19.26
	β	0.1	0.3	0.5	0.6	0.7
	mAP (%)	19.64	18.88	21.29	21.45	21.20

1. Hyperparameter Ablation

Ablation on BSPG Parameters. Our BSPG improves the reliability of pseudo-labels under point-level supervision through step-by-step smoothing. This reduces temporal jitter and mitigates boundary discontinuities (Fig. 2(c), Eq. 7). We ablate two key hyperparameters: the smoothing width w and the confidence decay factor β . As shown in Table 8, performance peaks at $w = 7$ (mAP: 21.45%), indicating that moderate neighborhood expansion effectively aggregates supervisory cues. Smaller windows ($w = 5$, mAP: 19.22%) under-smooth labels, whereas larger ones ($w = 9$, mAP: 19.26%) over-smooth and blur temporal boundaries. For the decay factor, optimal performance is achieved at $\beta = 0.6$. Lower values ($\beta = 0.1$, mAP: 19.64%) decay too quickly, limiting contextual information, whereas higher values ($\beta = 0.7$, mAP: 21.20%) overconfidently propagate pseudo-labels, introducing spurious activations. Overall, tuning both w and β improves pseudo-label quality and temporal localization.

Ablation on PSSC Parameters. Our PSSC enhances emotion boundary localization by leveraging the semantic space across temporal sequences, as illustrated in Fig. 2(c). The ablation study on the sample quantity in Eq. 5 is conducted based on $K = \lfloor T/k \rfloor$, where T denotes the total number of frames. This design accounts for significant temporal variations across input videos. As shown in Fig. 5, the hyperparameter k has a substantial impact on performance, with mAP showing a nonlinear trend. The best result (21.5% mAP) occurs at $k = 8$, indicating a balance between emotional coverage and noise suppression. A moderate sample count promotes the optimization of \mathcal{L}_{sc} by aggregating discriminative emotional patterns and capturing the spatial distribution of frame-level F_{mix} . In contrast, $k = 5$ yields insufficient cues, while $k = 12$ introduces redundancy.

Ablation on Loss Weights. We explore the impact of loss weights on the experiment in terms of mAP. As shown in Fig. 6, the blue curve indicates the variation of λ_1 when

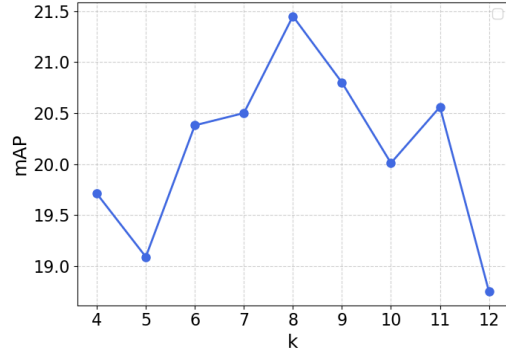


Figure 5. Ablation study of Top-K parameter k in PSSC on mAP performance.

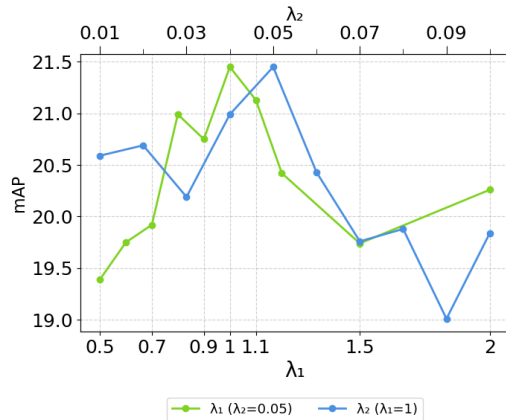


Figure 6. Ablation study of loss function weights λ_1 and λ_2 on mAP performance.

$\lambda_2 = 0.05$, while the green curve shows the variation of λ_2 when $\lambda_1 = 1$. The mAP reaches its peak at $(\lambda_1, \lambda_2) = (1, 0.05)$, highlighting the importance of properly balancing the two loss terms. Specifically, \mathcal{L}_{frame} improves the accuracy of emotion localization, whereas \mathcal{L}_{sc} helps align frame-level emotion segments. A small λ_1 results in insufficient boundary supervision, while an overly large λ_2 may over-constrain the alignment, leading to blurred segment boundaries and loss of fine-grained emotional cues.

2. Additional Results

Error Analysis. To gain deeper insight, we follow the error diagnosis protocol of [71] to break down the model outputs on the TSL300 dataset. As in Fig. 7, a key observa-

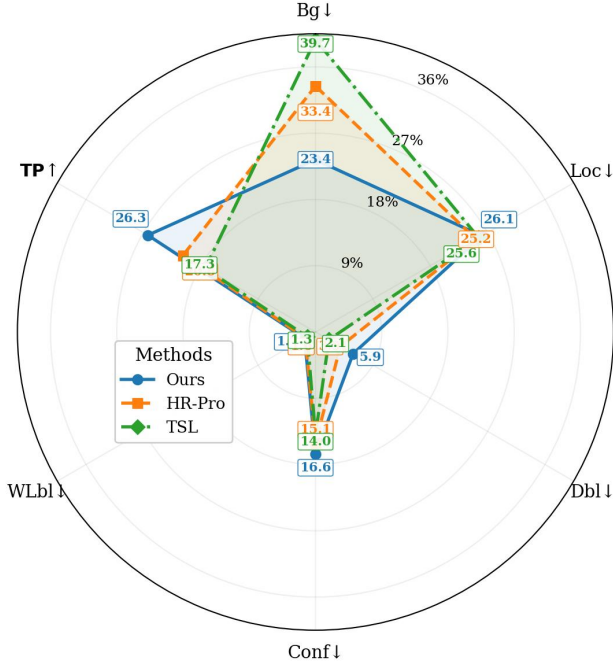


Figure 7. Proportion of proposal type for all prediction results of models on TSL300. Error categories: Bg (background), Loc (localization), Dbl (double detection), Conf (confusion), WLbl (wrong label), and TP (true positive).

tion is the substantial reduction in background errors, with a 10.0% decrease compared to HR-Pro (33.4% \rightarrow 23.4%) and a 16.3% decrease compared to TSL (39.7% \rightarrow 23.4%). This is accompanied by a notable increase in true positives (TP: 26.3%). These results strongly suggest that our approach effectively reduces false positives arising from background confusion. The fact that localization error (Loc) remains the dominant error type also indicates potential for further improvement in overall detection accuracy (mAP), pointing to future work on refining temporal boundaries.

PSSC Distance Metric Ablation. To assess the impact of different distance metrics on the identification of semantically relevant positive samples, we conduct an ablation study on the similarity function used in Eq. (4) of the PSSC module. Table 10 reports the mAP results under multiple IoU thresholds. Among the compared metrics, **Cosine similarity (Ours)** achieves the highest average mAP of 21.45%. In comparison, the L2 distance, the L1 distance and the dot product achieve lower scores of 20.29%, 20.05% and 21.00%, respectively. This corresponds to absolute improvements of 1.16%, 1.40%, and 0.45%. Under low IoU thresholds (0.1, 0.15, 0.2), where spatial constraints are loose and semantic disentanglement is more difficult, Cosine still achieves the best performance, with mAP of 29.31%, 25.47%, and 22.49%. These results demonstrate the effectiveness of cosine similarity in capturing semantic

Table 9. Performance comparison of different modality combinations on the TSL task. A: Audio, V: Visual, F: Local Face. Metrics are reported as mAP@IoU (%) across various thresholds and average mAP.

Modality	mAP@IoU (%)					Avg mAP
	0.1	0.15	0.2	0.25	0.3	
<i>Single Modality</i>						
A (Audio)	18.98	15.47	12.96	9.75	7.09	12.85
V (Visual)	19.27	16.14	12.06	9.14	6.45	12.61
F (Local Face)	22.11	15.97	11.33	8.40	6.62	12.88
<i>Bimodal Combinations</i>						
A + F	29.41	24.01	18.70	13.97	9.95	19.21
A + V	25.91	23.70	20.08	15.85	11.53	19.41
V + F	26.20	22.48	17.41	14.53	11.30	18.38
<i>Trimodal Combination</i>						
A + V + F	29.31	25.47	22.49	16.76	13.24	21.45

relationships between feature vectors.

Table 10. Ablation of feature distance metrics for Point-aware Sentiment Semantics Contrast modeling.

Method	mAP@IoU (%)					Avg mAP
	0.1	0.15	0.2	0.25	0.3	
L2	28.06	24.40	20.98	16.49	11.55	20.29
L1	26.53	23.66	20.70	16.36	12.97	20.05
Dot	27.23	24.90	21.21	17.42	14.22	21.00
Cosine(Ours)	29.31	25.47	22.49	16.76	13.24	21.45

Modality Combination Analysis. We conduct an ablation study to examine the impact of the modality information, as shown in Table 9, which reports the performance of different modality combinations. Among the unimodal inputs, the face embedding (F) achieves the best performance (mAP: 12.88%), slightly outperforming the audio (A) and visual (V) features. This suggests that each modality provides complementary yet insufficient information when used in isolation. Bimodal combinations such as A+V and A+F yield significantly improved results (mAP: 19.41%, representing an increase of 6.56%; and 19.21%, with an increase of 6.36%, respectively). These results indicate strong complementarity between audio and visual/facial cues. Meanwhile, the relatively lower performance of V+F (18.38%) may be attributed to redundancy between holistic and local visual features. Trimodal fusion (A+V+F) further boosts the performance to 21.45% mAP, demonstrating the advantage of integrating heterogeneous modalities.